Dissolved air flotation of Chlorella sp. using chitosan: influence of algal organic matter and growth phase on coagulant dose

Peer-reviewed author version

PAPPA, Michaela; LAMA, Sanjaya; Demir, Irem; VARAS PEREZ, Paula; ADRIAENSENS, Peter; MARCHAL, Wouter; Formosa-Dague, Cécile & VANDAMME, Dries (2025) Dissolved air flotation of Chlorella sp. using chitosan: influence of algal organic matter and growth phase on coagulant dose. In: Algal research, 89 (Art N° 104028).

DOI: 10.1016/j.algal.2025.104028
Handle: http://hdl.handle.net/1942/45987

Dissolved air flotation of Chlorella sp. using chitosan: influence of algal organic matter and growth phase on coagulant dose

Michaela Pappa, Sanjaya Lama, Irem Demir, Paula Varas Perez, Peter Adriaensens, Wouter Marchal, Cécile Formosa-Dague, Dries Vandamme

PII: S2211-9264(25)00137-7

DOI: https://doi.org/10.1016/j.algal.2025.104028

Reference: ALGAL 104028

To appear in: *Algal Research*

Received date: 16 December 2024

Revised date: 4 April 2025

Accepted date: 6 April 2025

Please cite this article as: M. Pappa, S. Lama, I. Demir, et al., Dissolved air flotation of Chlorella sp. using chitosan: influence of algal organic matter and growth phase on coagulant dose, *Algal Research* (2025), https://doi.org/10.1016/j.algal.2025.104028

Dissolved air flotation of *Chlorella* sp. using chitosan: influence of algal organic matter and growth phase on coagulant dose

Michaela Pappa[a], Sanjaya Lama[a], Irem Demir[b,*], Paula Varas Perez[a], Peter Adriaensens[a], Wouter Marchal[a], Cécile Formosa-Dague[b], Dries Vandamme[a**]

[a] Analytical & Circular Chemistry, Hasselt University, Agoralaan building D, Science Tower, 3590 Diepenbeek, Belgium

[b] Toulouse Biotechnology Institute, Université de Toulouse, INSA, INRAE, CNRS, Toulouse, France

[*]present affiliation : UCLouvain, Université catholique de Louvain, Louvain-la-Neuve, Belgium

[**]corresponding author: dries.vandamme@uhasselt.be

Abstract

This study investigates the efficient separation of *Chlorella* sp. microalgae using dissolved air flotation with chitosan as a coagulant. Improving the harvesting process, which significantly contributes to total costs and carbon footprint, could lead to competitive microalgae products and commodities. The exponential phase required 0.20 $mg \cdot mg^{-1}$ chitosan, which is almost two times more than the chitosan dose of 0.12 $mg \cdot mg^{-1}$ required for the stationary phase of growth, although the algal biomass concentration had increased from 0.26±0.06 to 0.53±0.01 $mg \cdot L^{-1}$ and the concentration of algal organic matter from 8 to 32 mg $C \cdot L^{-1}$ in dissolved organic carbon, respectively. It is also shown, *via* Microscope Force Spectroscopy, that the cell measured directly from the culture had bound algal organic matter to their surface at pH 8.5, increasing their softness (Young's Modulus=8.1±10 kPa), roughness (4.2±2.4 nm) and interaction with bubbles (2.5±2.1 nN, adhesion 64.4%), compared to the washed cells in PBS buffer at pH 7.4 (1474±1053 kPa; 1.3±0.4 nm; 0.8±0.5 nN, adhesion 9.1%, respectively). Polysaccharides, mainly containing arabinose (29.2±6.9% and 33.0±1.7% dw polysaccharide) and galactose (34.2±8.1% and 17.43±1.3% dw), while acidic residues of the polysaccharides (6.7±2.1% and 13.1±5.8% Area) were also present along with protein (9.1±2.2% and 0.9±0.2% dw AOM) in exponential and stationary growth phase, respectively. Nevertheless, the relationship between AOM composition and its underlying structure and functionality is not yet fully understood.

Keywords

Microalgae; Flocculation; Cationic polyelectrolyte; Bridging; Extracellular Polymeric Substances; Dewatering

List of abbreviations

Coagulation: C
Dissolved Air Flotation: DAF
Algal Organic Matter: AOM
Exponential growth phase culture in the absence of AOM: exp.AOM-
Exponential growth phase culture in the presence of AOM: exp.AOM+
Stationary growth phase culture in the absence of AOM: stat.AOM-
Stationary growth phase culture in the presence of AOM: stat.AOM+
Separation efficiency: η
Zeta-potential: ζ
Dissolved organic carbon: DOC
Dissolved total nitrogen: DTN

1 Introduction

Microalgae are established as one of the most prominent types of biomass due to their functionality, eco-friendliness, and potential for bioproducts [1]. As global challenges of resource scarcity and environmental impact escalate, the search for economic alternatives becomes crucial [2]. Microalgae's diverse applications, from waste treatment to nutritious low-water footprint food sources and drugs, underline its significance. However, operational efficiency demands a simultaneous cost reduction and increased revenue [3–5].

Harvesting the microalgae is one of the most divisive steps and greatly influences the overall process's costs [6]. There is no universal treatment to achieve a cheap concentration of the microalgae culture from the dilute suspension – similar to water – to a slurry consistency (up to 25% solids) [7]. However, coagulation is a popular primary step among the different available techniques. This process allows the formation of larger aggregates that are easier to separate from the medium. However, conventional coagulants often contain metal-based compounds or toxic substances that contaminate the biomass and minimize its potential applications [8,9]. These challenges have prompted the exploration of bio-polymers and green coagulants as alternatives, and to integrate them into biotechnological approaches by studying their interactions and mechanisms [10].

Chitosan is a popular coagulant usually produced by alkaline treatment of the chitin-rich exoskeleton of crustaceans or fungi [11]. It is a cationic linear polysaccharide composed of random residues of β-linked D-glucosamine and N-acetyl-D-glucosamine with three different polar functional groups; hydroxyl, ether, amide and amine groups [12]. The C2 ammonium group's positive charge decreases with increasing pH [13,14], and has a pK_a of ~6.5 [15]. Chitosan flocculation has been described at low pH as a rapid 'non-equilibrium' bridging process [16]. When added to a solution with high concentration of particles and low ionic strength, it will adopt an extended conformation that will allow interactions *via* charge neutralization along its length with oppositely charged constituents. During stirring, the neutral patches on the cells reduce the repulsion. The cells can then interact with other cells that are still negatively charged. Chitosan realigns and interacts with new cells in a never ending repetition [11,15,16]. At high pH (> 7.5), there is partial deprotonation of the ammonium groups and chitosan precipitates (sweeping) and traps the constituents [17–21]. Deprotonation of the ammonium group reduces the charge density. It allows the chitosan molecules to fold and re-establish their "extensive intra and intermolecular" hydrogen bonds between the amine groups

[12]. In neutral pH 6-8, a combination of these mechanisms is expected; electrostatic adsorption bridging and hydrogen bonding interaction with the culture's constituents and other chitosan molecules allow for their interconnection. Interestingly, atomic force microscopy (AFM) tests have reported that specific interactions take place between chitosan and cell surface polysaccharides of *Chlorella vulgaris* [20].

In microalgae cultures, such interactions extend beyond chitosan and cells, and also involve extracellular organic compounds during cultivation, referred to as Algal Organic Matter (AOM). The AOM composition is dynamic and reactive to environmental stressors. It accumulates over time, creating a unique biological system for different species, cultivation conditions, and growth phases. Generally, AOM has an overall negative zeta potential (ζ) and can influence the separation in different ways via its interactions with the cells and the coagulant [22–25]. If AOM is non-ionic, the higher its molecular weight (MW) the more it hinders coagulation. If AOM is ionic, both its MW and concentration influence coagulation [26]. Low MW AOM will increase proportionally the negative charges of the solution and the particles, which will create a stable suspension and increase the coagulant demand for its discharge [24,26,27]. Similarly, large MW ionic AOM in high concentration (> 2 $mg \cdot L^{-1}$) hinders coagulation because it completely covers the cell's surface with negative charges [26]. Yet, in low concentrations, it acts as a coagulant aid, which means that the AOM partially chemisorbs on the cell surface and extends to the surrounding area, which facilitates interactions [26]. Additionally, it has been described that large MW AOM creates an increased-viscosity solution which supports separation [24,26,28].

Coagulation is usually followed by sedimentation, centrifugation, filtration, or flotation, each of which has its advantages and disadvantages. Combining coagulation, followed by dissolved air flotation (CDAF) is common practice for an enhanced rapid separation [29]. In dissolved air flotation (DAF), microbubbles are produced, via the release of air-saturated water [30], that collide and adhere to the flocs. Briefly, their attachment is achieved when they reach a critical distance where attractive forces (*i.e.*, Van der Waals, electrostatic, and hydrophobic) can overcome the repulsive forces (*i.e.*, hydrodynamic retardation, electrostatic, and hydrophobic-hydrophilic) [31–33]. Then, the flocs can float to the surface and create a foam layer, which is skimmed or overflowed to a second tank [7]. DAF is usually selected for microalgal culture harvesting because of its rapid and efficient in-line production capability for large volumes in limited space, while highly concentrating the biomass and preserving cell integrity [30,34].

The bubble characteristics, *i.e.* size, charge, etc. influence the bubble-floc attachment efficiency. Normally, the bubble's air-water interface has a negative charge (-25 mV in neutral pH 6-8), electrostatically repelling the culture constituents [13,35], and could potentially interact *via* hydrophobic interactions. Coagulants reduce the charge density of the cells and AOM, and aggregate them, increasing their size. They allow the attractive Van der Waals forces and hydrophobic interactions to overpower the electrostatic repulsion and the short-range hydrodynamic interaction (physical obstacle of water between two particles), facilitating collisions and attachment [35,36].

Valorizing biopolymers as biocoagulants, for example, based on cellulose or starch [37,38], for harvesting the microalgal biomass is increasingly favored over traditional coagulants, such as metal salts, and synthetic coagulants that have harmful implications for human consumption and the environment [39,40]. Furthermore, biopolymers are biodegradable and are extracted from biomass sources that are abundant on Earth [37,41]. Chitosan is a promising candidate among biopolymers for microalgae coagulation, which diverges from other polymer coagulants regarding water chemistry. Namely, it has a primary amine group, and thus, differs from other popular polysaccharide-based and tannin-based biocoagulants, which are commonly grafted with quaternary ammonium groups [20,39]. It is generally accepted as biocompatible, and non-toxic for pharmaceutical applications [42] and human consumption [43,44]. Therefore, there is to date no indication that chitosan would limit the valorization of microalgae biomass and products [12,37,39,40,45–47]. However, chitosan's exhibits antibacterial properties that can impact the cell wall integrity of some cyanobacteria [48–50]; yet, in green microalgae, chitosan has not been shown to damage the cell wall integrity, or have follow-up implications for medium re-use or final products to these authors' knowledge [51,52].

The existing literature predominantly emphasizes chitosan's role in coagulation-flocculation [20,39]. However, there is a critical gap in understanding the implications of using chitosan in flotation separation [53] of eukaryotic microalgae considering the dynamics and interactions between chitosan, the cells, the AOM, and how the formed flocs will interact with bubbles in different growth phases. Comprehensive studies are imperative on chitosan interactions with the AOM, which can be diverse according to species and culture conditions, as well as the bubbles in CDAF. Finally, more research is required to understand the AOM constitution with its role and characteristics, not only providing insights for the separation of the biomass but also to unlock its full potential in advanced applications.

In this study, *Chlorella* sp. is cultivated on a laboratory scale to investigate the effect of the growth phase (exponential versus stationary) on the separation efficiency *via* chitosan coagulation dissolved air flotation. The cell characteristics and the AOM concentration and composition in the exponential and stationary growth phases were analyzed and linked to the dose-response of chitosan in CDAF.

2 Materials and Methods

2.1 Culture growth

The freshwater green microalgae *Chlorella* sp. (kindly provided by CNEA, Universidad de Oriente, Cuba) was cultured in modified BG11 medium [54] in 25 L tube photobioreactors exposed to white led light of total luminous intensity of 2820 cd (HVPAqua, the Netherlands) in light: dark ratio of 16:8 hours. The nitrogen source was adapted to 1.37 $mg \cdot L^{-1}$ $NaNO_3$ to achieve nitrogen limitation within the first eight days of growth (Thermo Scientific Dionex ICS-6000, Column: Dionex IonPac AS14A (4×50mm) & AS14A (4×250 mm)). The pH was maintained at 8.0 ± 0.5 with the help of a pH-stat system *via* the external addition of CO_2 gas. The microalgae culture was cultivated to the mid-exponential phase (day 5-7) and mid-stationary phase (day 20-25) with dry weight biomass of 0.26 ± 0.06 $g \cdot L^{-1}$ and 0.53 ± 0.01 $g \cdot L^{-1}$ (±10%) dry weight biomass, and approximately 8 and 32 ppm dissolved organic carbon (DOC) (TOC-L_{CPH}, Shimadzu Benelux), respectively (**Section A.2**) [55,56]. The setup dimensions, the culture follow-up methods and characteristics have been summarized in Supporting Information (**Section A.2**).

2.2 Coagulation and Dissolved Air Flotation Protocol

The microalgal biomass grown to exponential or stationary phase was separated by centrifugation (disc stack centrifuge, 8000 rpm, Milky Day. Czech Republic). Then, it was resuspended in fresh BG11 medium (AOM-) or its spent BG-11 medium, rich in algal organic matter (AOM+). The biomass concentration is determined by absorbance measurements at 750 nm (Ultraspec-7000, GE) (Absorbance = 3.3458*(Dry weight concentration) + 0.1702, R^2=0.947). The pH was adjusted to 8.0 with 1M NaOH or 1M HCl (Knick pH-Meter 764 Multi-Calimatic) and divided into 1 L aliquots. The chitosan (100-300 kDa, Deacetylation Degree >99%, Acros Organics) was dissolved in 0.04 M HCl to achieve a 5 $g \cdot L^{-1}$ stock solution [18].

The Coagulation and Dissolved Air Flotation (CDAF) jar testing was conducted using the Platypus DAF Jar Tester (Platypus DAF jar tester, Aquagenics Pty Ltd, Australia; [57]). The setup is described in **Section A.1**. The 1 L aliquots were added to the DAF jars, and the appropriate dose of chitosan was added at the beginning of the intense stirring phase, also referred to as the homogenization phase, which lasted for 10 min at 200 rpm. Then, a slow stirring phase followed to allow the flocs to grow for 20 min at 20 rpm. The final concentration of chitosan for the exponential phase was 0.00 to 0.51 $mg \cdot mg^{-1,}$ and for the stationary phase,

0.00 to 0.31 mg·mg^{-1} chitosan per dry weight biomass. Finally, the pressurized air at 450 kPa was allowed in the jar with a 31% recycle ratio, a dilution factor of 1.45 (see **Fig. A.1**). A sample of 100 mL from the subnatant was kept to calculate the separation efficiency and further analyses 7 min after the start of the DAF step. A small portion was first dispensed to retrieve a representative sample since flocs were trapped in the neck of the tap. The zeta potential (ζ) (Zetasizer Nano, Malvern, UK) and absorbance were measured. The separation efficiency (η) % was calculated as the difference of the initial absorbance at 750 nm compared to the final absorbance:

$$\eta(\%) = \frac{OD_i - OD_f \cdot 1.45}{OD_i} \times 100\% \qquad (1)$$

where OD_i is the initial and OD_f is the final absorbance of the aliquots [58].

The resulting points were fitted *via* the Boltzmann sigmoidal regression function (Origin 2020; variables are described in Appendix A), similarly to Lama et al. [58]. The restabilization points showcase the end of the sigmoidal regression trend of the data, where excess of chitosan coagulant causes a decrease in separation efficiency, were not included.

2.3 Atomic and Fluid Force Microscopy (AFM and FluidFM)

Cells from stationary phase cultures were immobilized on a positively charged glass slide (Superfrost™ Plus adhesion, Epredia, USA), either directly (unwashed) or after a washing step in PBS using centrifugation (3000 g, 3 min, five times; washed) [59,60]. For that, 1 mL of the washed or unwashed cell suspensions were deposited on the glass slides, allowed to stand for 30 minutes, and rinsed using PBS buffer at pH 7.4. Images of the cells were obtained using the Quantitative Imaging (QI) mode available on the Nanowizard IV XP AFM (Bruker, USA), with MSCT cantilevers (Bruker, nominal spring constant of 0.01 N·m^{-1}). QI images were acquired with a resolution of 100 × 100 pixels, an applied force <1.0 nN, and the constant approach/retract speed was 120 µm·s^{-1} (z-length of 2 µm). High-resolution images were directly obtained on top of the cells of small areas (1 × 1 µm) using AFM in contact mode, with MSCT cantilevers (Bruker, nominal spring constant of 0.01 N·m^{-1}), using a resolution of 512 lines and a speed of 4 Hz. The average roughness Ra was then calculated from these images using the Data Processing Software (Bruker, USA); 11 washed cells and 9 unwashed cells in total were analyzed. The force spectroscopy mode was used to acquire force curves on 1 × 1 µm areas on top of cells to determine the cell's Young modulus, using an applied force ranging from 0.5 to 2 nN, with MSCT cantilevers (Bruker, nominal spring constant of 0.01 and 0.03 N·m^{-1}). For

each cell, arrays of 20 × 20 force curves were recorded. The Young's modulus values were then calculated by fitting each force curves converted into indentation curves with the Hertz model [61] in the Data Processing software (Bruker, USA), as described in [62]. In this case also, 10 washed cells and 7 unwashed cells were analyzed. For washed cells, an indentation segment of 50 nm was used, while for unwashed cells, it was of 250 nm.

Finally, to determine cell surface hydrophobicity, the method developed in [63] was used. It consists of using FluidFM (Cytosurge AG, Switzerland) to produce a stable bubble at the aperture of a micropipette cantilever (Cytosurge AG, Switzerland, aperture of 8 µm, nominal spring constant of 0.3 and 2 $N \cdot m^{-1}$), and probe its interactions with cells in force spectroscopy mode. Prior to the experiments, FluidFM probes were functionalized with self-assembled monolayers of silanes. To perform these experiments, arrays of 20 × 20 curves were recorded on small areas of 1 × 1 µm on top of cells, using an applied force of 1 nN, a z- length of up to 3 µm and a constant retraction speed of 3.0–6.0 $\mu m \cdot s^{-1}$. The force curves obtained were then used to determine the maximum adhesion force using the Data Processing Software (Bruker, USA). In this case, 11 washed and 13 unwashed cells were analyzed. For all the experiments described, the spring constant of the cantilevers used (including the microfluidic cantilevers used with FluidFM) was determined before measurement using the thermal noise method [64].

2.4 Algal Organic Matter analyses

The AOM samples were retrieved by centrifugation (disc stack centrifuge, ~5000 g, Milky Day, Czech Republic). The microalgal culture was centrifuged four consecutive times until the supernatant came out clear and was freeze-dried. The dry AOM was dissolved in a small amount of double distilled water with four cycles of magnet stirring (400 rpm, 30 min) and sonicating (45 Hz, 180 W, 15 min, VWR Ultrasonic Cleaner USC - THD) till the particles were completely dissolved. The exponential phase AOM required twice the amount of water to dissolve, while stationary AOM was able to dissolve in a concentration of 10 $mg \cdot mL^{-1}$. These solutions were dialyzed with 1 kDa dialysis membrane (Spectra/Por® 6, 514-0942, VWR). The main contributor of the ash content in untreated AOM of the exponential phase was the medium's salts, which interfered with the spectrophotometric analyses, forming precipitates. The ash content, before and after dialysis, was quantified *via* thermogravimetric measurements [65] up to 950 °C, and was reduced by approximately 85%. The conductivity (inoLab Cond 7110) decreased by one order of magnitude for all treatments (≤100 $\mu S \cdot cm^{-1}$). The solution was then freeze-dried and stored at -20 °C till further analysis.

The dialyzed-lyophilized AOM was dissolved in water at 80 $mg \cdot L^{-1}$ and 20 $mg \cdot L^{-1}$ dry AOM for the exponential and stationary phase, respectively, and DOC, dissolved total nitrogen (DTN), and ζ were measured in a pH range 4-10. The pH was adjusted using 1M HCl and 1 M NaOH.

Fourier–transform infrared spectroscopy (FTIR) was performed on the dry AOM with a diamond crystal (PIKE, Fitchburg, USA) in attenuated total reflection, similarly to Lama et al. [66] (Vertex 70 spectrometer with a deuterated triglycine sulfate detector, Bruker, Karlsruhe, Germany). The spectral region was 4000–600 cm^{-1} with a resolution of 4 cm^{-1} (32 scans per sample).

The dry AOM 1.00 ± 0.05 mg was hydrolyzed with 5 mL 2 N trifluoroacetic acid (TFA) in a tightly closed 10 mL pyrex tube with septum on a heat block at 100 °C for 1 h for quantification of the total and composition of monosaccharides (triplicate) [67]. The TFA was evaporated at 40 °C under nitrogen gas flow till the sample was completely dry and then dissolved in 1 mL double distilled water. An aliquot of the solution was used to measure the total monosaccharides with the MBTH method (NREL) [68,69], while the rest was diluted appropriately and filtered to be injected in a HPAEC-PAD (ICS-6000 Dionex system, guard column (3 × 50 mm) and CarboPac PA20 column (3 × 150 mm), Thermo Fisher Scientific), for monosaccharide composition analysis, which followed the eluent composition and gradient profile, previously described in Nagel et al. [70].

AOM samples of 9.92 ± 0.02 mg were digested with 1 mL 1M HCl and then the total amount of sulfate groups was quantified using the turbidimetric assay of the barium chloride-gelatin method [71,72]. From the digestate, an aliquot of 0.1 mL was used for the assay (all quantities were halved [71,72]), and the turbidity was measured with a microcuvette at 360 and 500 nm for three replicates.

Protein was quantified *via* the Lowry assay [55]. Samples were weighed at 5.00 ± 0.05 mg per replicate in a 15 mL centrifuge tube (triplicate), and the protocol was followed with no deviations.

The dry and dialyzed AOM approximately 80 mg for the exponential phase and 20 mg for the stationary phase were mixed with 7 mL dichloromethane (CAS 75-09-2, UniSolv®, Merck) in a glass centrifuge tube with screw cap to extract non-polar compounds. The samples were vortexed thoroughly before sonication (45 Hz, 10 min). This process was repeated 6 times in the time period of 3 hours, after which the mixture was centrifuged (8 min 3000 g), and the

supernatant was transferred to a new vial. The residue was resuspended in another 7 mL of dichloromethane and after thorough mixing, they were centrifuged once more. The supernatant was transferred to the vial with the extract.

The dichloromethane extracts of the dry dialyzed AOM were evaporated under a gentle stream of nitrogen to a volume of 40 to 50 µl and thereafter transferred to an Eco-Cup SF (PY1-EC50F, Frontier Laboratories LTD, Japan). 5 µl of a 25% tetramethylammonium hydroxide solution in methanol (25 wt% in methanol, CAS 67-56-1, Acros Organics) was added to the cup, for in situ esterification, which was then evaporated to dryness, following the method described in Hardell et al. was followed [73]. The extracts were analyzed using the pyrolysis technique combined with gas chromatography /mass spectrometry (PY-GC/MS). The analysis was performed with an EGA/3030-D Multi-Shot Pyrolyzer (Frontier Laboratories LTD, Japan) and a Trace 1300 gas chromatograph (Thermo Scientific, USA) equipped with an Ultra ALLOY-1 capillary column (UA1-30M-0.5F, 30 m length, 0.25 mm I.D., film thickness 0.5 µm, Frontier Laboratories LTD, Japan) coupled to an ISQ 7000 single quadrupole mass spectrometer (Thermo Scientific, USA). The cups were transferred into the pyrolysis module where they were heated for 0.2 minutes at 400°C. The pyrolyzates were introduced into the capillary column with a 1/80 split, after which the following temperature program was started; the column temperature was maintained at 35°C for 1 min and raised to 320°C at a rate of $10°C \cdot min^{-1}$ and a final hold time of 2.5 min. The injection port was set at 300°C and the MS transfer line at 280°C. Helium was used as carrier gas and the flow rate was set at 1 $mL \cdot min^{-1}$. The mass spectrometer was operated in electron ionization mode with 70 eV at a source temperature of 300°C and a mass range of 33-550 m/z with a scan time of 0.2 sec. Data processing was performed using Chromeleon 7.3 (Thermo Scientific, USA).

2.5 Statistical Analysis

In addition to sigmoidal Boltzmann regression for all dose-response results, comparison of datasets was performed, and student's t-tests were employed on the AOM analyses results and AFM measurements (Origin 2020). The AOM analyses results represent the average of triplicate measurements, unless it is mentioned otherwise. Significance was determined at $p < 0.1$ (Section A.3).

3 Results and Discussion

Coagulation and Dissolved Air Flotation (CDAF) was applied to a *Chlorella* sp. culture using chitosan in exponential and stationary phase, both in the presence (AOM+) and absence of AOM (AOM-) (**Fig. 1**). The four dose-response curves for separation efficiency (η) (**Fig. 1A)** and zeta potential (ζ) of the subnatant after the separation (**Fig. 1B**) are depicted as a function of chitosan dose. Comparison of the dose-response curves allowed the following observations:

- In the absence of AOM, the chitosan dose required, when normalized by weight, was similar to reach comparable separation efficiencies. Thus, cell growth phase did not seem to affect the separation process.
- In the presence of AOM in the exponential phase, the coagulant demand increased by 100%, inferring that AOM interacts with the coagulant.
- In the presence of AOM, in the stationary phase, accumulation of AOM did not proportionally inhibit separation efficiency, which suggests that the AOM is different in quantity and/or composition, thus interacting differently compared to the exponential phase.
- In the stationary phase, there was increased separation even in the absence of chitosan, which can indicate that the AOM is different in the two growth phases.

In the following subsections, these observations are elaborated, correlating separation behavior with pH, charge neutralization, intermolecular forces and composition information, in order to deeper understand the underlying (physico)chemical mechanisms.

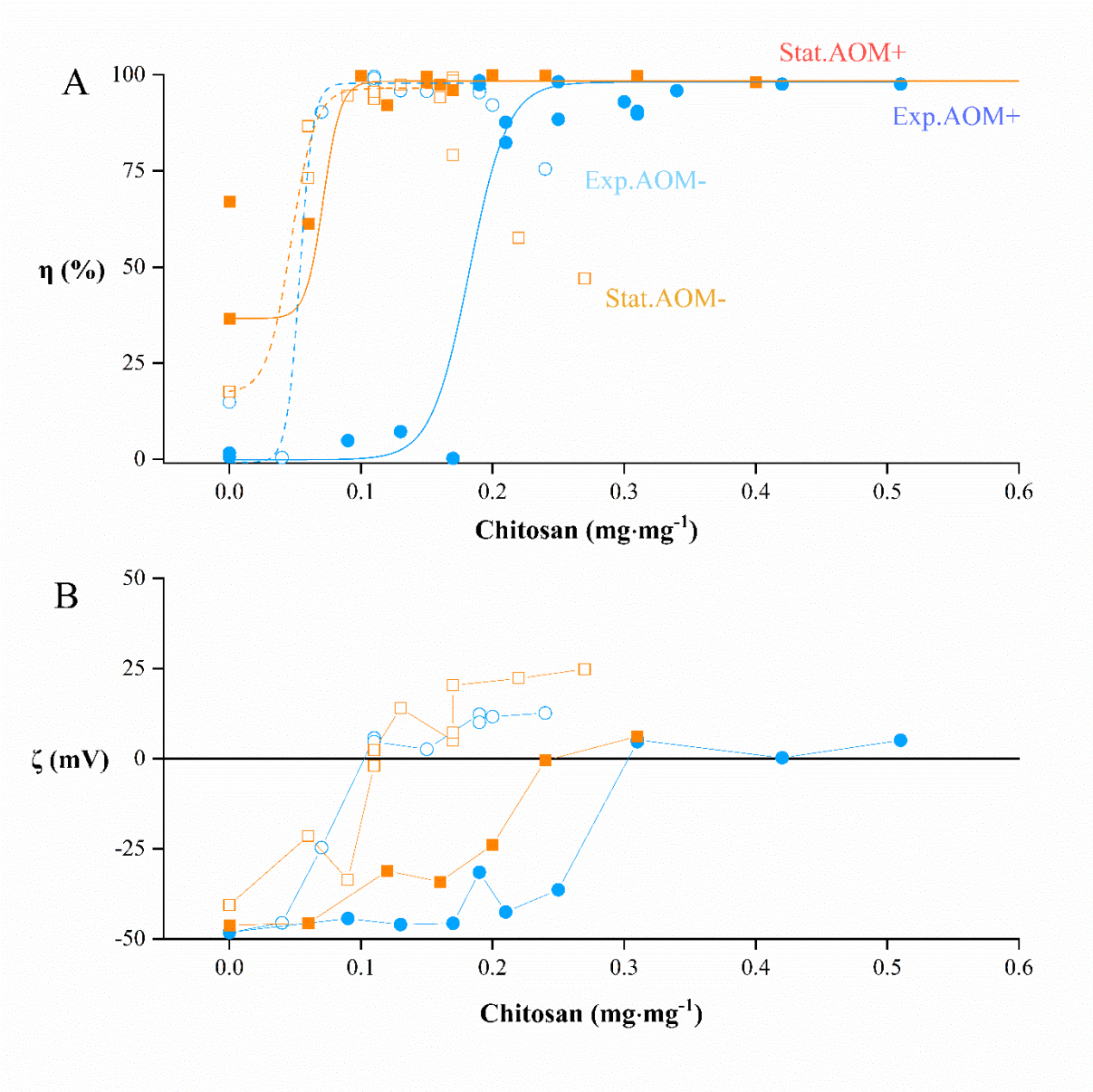

Figure 1. The response of increasing doses of chitosan coagulant (mg·mg^{-1} biomass) to the separation efficiency η% (A) fitted by Boltzmann sigmoidal regression (Origin 2020; variables are described in Appendix A), and zeta potential ζ (B). The samples evaluated were the cultures in the exponential phase in the absence (-○- Exp AOM-) and presence of AOM (-●- Exp AOM+) as well as the culture in the stationary phase in the absence (-□- Stat AOM-) and presence of AOM (-■- Stat AOM+), with R^2 of 0.998, 0.999, 0.995 and 0.985, respectively.

3.1 In the absence of AOM, the separation efficiency is independent of the cell growth phase.

It is apparent that the separation efficiency (η) is not affected by differences in cell characteristics in the exponential and the stationary growth phase. The culture in the exponential phase in the absence of AOM (Exp.AOM-) resulted in high η (90%) with a low chitosan dose (0.07 mg·mg^{-1} biomass). Increasing the dose resulted in maximum separation of 99% with 0.11 mg·mg^{-1} biomass of chitosan, but a further increase in dose negatively affected separation, causing restabilization due to repulsion among the now positively charged cell surface (charge reversal) (**Fig. 1A**, **Fig. 2**). The zeta potential (ζ) measurements of the subnatant confirm this since, at the optimum point, the value was 5.8 mV and increased to over 10 mV for overdosing at 0.20 and 0.24 mg·mg^{-1} with efficiencies of 92% and 76%, respectively (**Fig. 1B**). The flocs formed at the optimum dose rose in isolated patches, some of which sedimented and thus the foam formation is described as weak and unstable (**Fig. 2, Fig. A.2**). A possible explanation would be that their large size and extensive structure resist the rising gradient [74], and not enough bubbles were attached to the floc to keep its mass afloat (**Fig. 2B**).

In the Stat.AOM- phase, the separation efficiency followed a similar trend as the culture in the Exp.AOM-phase. There was 73% separation with 0.06 mg·mg^{-1}, and a maximum efficiency of 97% was obtained with 0.13 mg·mg^{-1}, 0.02 mg·mg^{-1} difference compared to Exp.AOM-. (**Fig. 1A**). Similarly, overdosing resulted in lower separation, with the ζ increasing over 20 mV (**Fig. 1B**), yet the foam layer had better homogeneity than its exponential counterpart (**Fig. 2C, Fig. A.2**).

Hence, the cell growth phase does not influence the separation efficiency in the absence of AOM, and the differences in cell physiology have a negligible impact, pointing to a state in which chitosan is bridging cells without completely neutralizing their negative charges.

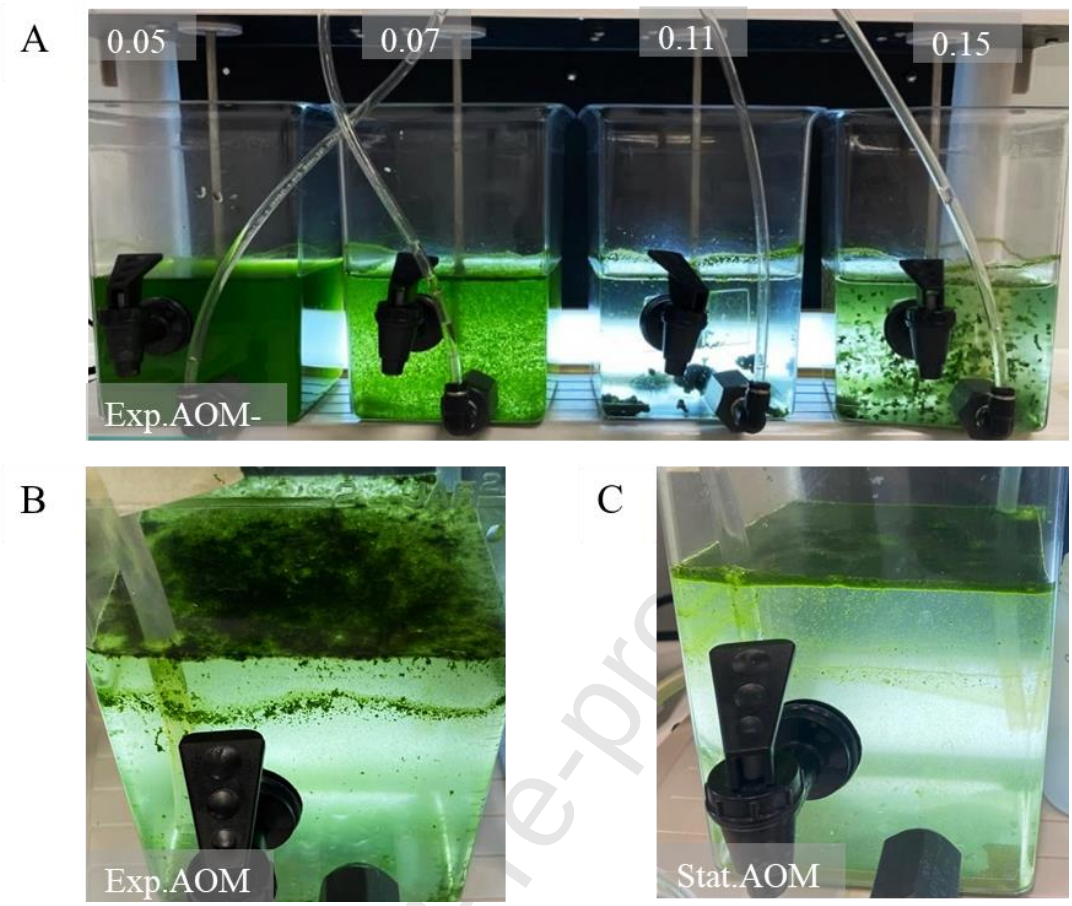

Figure 2. *Chlorella* sp. jar tests in the exponential phase culture showcasing: A. The restabilization phenomenon in the absence of AOM with 0.05, 0.07, 0.11, 0.15 mg·mg^{-1} biomass, during the slow stirring step, B. the patchy foam formation in the absence of AOM and C. the homogenous foam layer in the stationary phase in the absence of AOM.

3.2 The AOM influences separation efficiency differently in the exponential and stationary phase

In the exponential phase, η is negatively affected by the presence of AOM (Exp.AOM+). There was no separation up to chitosan dosage levels of 0.20 mg·mg^{-1}, where a steep increase to η=92% is found, corresponding to approximately double the coagulant demand with respect to the chitosan dose in the absence of AOM (Exp.AOM-). This shows that the AOM plays an inhibitory role in the separation in the exponential phase, as it has been inferred in several *Chlorella* strains [75]. Specifically, it has been discussed in several publications by Bernhardt, Henderson, Pivokonsky, and their coworkers that AOM concentration as a ratio to the cell surface area affects coagulation [76–78]. A high concentration of anionic AOM (> 2 mg·L^{-1}) leads to complete coverage of the cell surface, increasing charge density and inhibiting aggregation [26], like in the exponential phase, which is no longer evident in the stationary

phase. Furthermore, high pH has been inferred to be beneficial for chitosan coagulation. The corresponding final pH of 7, signifies that a part of the functional groups of the cells [79], and AOM [23], are deprotonated, and only a fraction of the chitosan's amine groups has positive charges (pH= 7 > pK_a=6.5), which is also important for coagulation.

Additionally, overdosing did not cause restabilization and plateaued at high η (≥90%), (**Fig. 1A**). Correspondingly, the ζ was below -30 mV until the 0.34 mg·mg^{-1} dose, from which dose it remained slightly positive (**Fig.1B**). The absence of restabilization has been previously attributed to the presence of high molecular weight (MW) AOM, larger than 500 kDa, for *Microcystis aeruginosa* because they mitigate electrostatic repulsion. Yet, restabilization was observed for *C. vulgaris,* in the same study which only had 5% of its AOM larger than 500 kDa [28]. Nevertheless, the presence of AOM in the stationary phase did not inhibit η, even though there is four times the amount of AOM in the culture. There was a gradual increase in separation, reaching 92% at 0.12 mg·mg^{-1}, and stabilized around 99% for chitosan doses of 0.15 mg·mg^{-1} and higher. Improved separation with *Chlorella* sp. of late exponential and early stationary phase cultures compared to exponential phase cultures has been previously reported in different studies: Al^{3+} CDAF [49], with $AlCl_3$ sedimentation [50], and chitosan sedimentation, similarly, achieving 99.0% separation with 50% less chitosan in the stationary phase [51]. In the current study, the ζ remained below -20 mV up to 0.20 mg·mg^{-1} chitosan and became positive if the dose was more than 0.24 mg·mg^{-1} (**Fig. 1B**), while the pH decreased below 7, which would enrich the chitosan molecule with positive charges facilitating attracting electrostatic interactions with the cells. In both growth phases, when AOM was present, the ζ of the solution remained negative till high dosages, becoming slightly positive only for the highest chitosan concentration. Further chitosan addition would probably restabilize the suspension due to excess positive charges and cause repulsion of the particles. However, one would need to overdose greatly to reach that point. In larger-scale application, this experimental set-up requires less stringent control due to the wide stability – chitosan span. It is important to not exceed the optimum ζ "operational window" during coagulant addition, which for *C. vulgaris* was between -10 to +2 mV, independent of pH and required more coagulant than other microalgae [77]. It seems that this ζ window is broader for the current *Chlorella* sp. but the value changes gradually in the presence of AOM (**Fig. 1B**).

Literature on the flotation separation of *Chlorella* sp. is extensive; Demir-Yilmaz et al. achieved around 60% separation of *C. vulgaris* biomass in the exponential phase using polyoctyl-chitosan as a bubble modifier [60]. Zhang et al. reached 81% separation of *C.*

zofingiensis in the exponential phase with 0.07 mg·mg^{-1} chitosan CDAF [80]. Relatively, the current study's *Chlorella* sp. culture has achieved at least as efficient separation with the chitosan CDAF process in the stationary phase of growth. Notably, Cheng et al. separated low-concentration *M. aeruginosa* culture with Al^{3+} bubble modification and observed a positive effect for η at low AOM concentrations, referring to a "protein-originated network" [53]. However, inhibition at high concentrations (>10.71 mg C·L^{-1}) could not be overcome with higher Al^{3+} modifier concentration increase.

Since there is a different influence of the AOM in the exponential and stationary phase, it can be inferred that the AOM has a different composition and/or concentration in the two phases. Analyses showed that the stationary phase had four times more AOM (~32 mg C·L^{-1}) than in the exponential phase (8 mg C·L^{-1}) (**Table 1**). Thus, the amount of AOM expressed in mg C·L^{-1} does not proportionally affect its interaction during coagulation and flotation. In the literature, various species within the *Chlorella* genera, have been documented to produce varying amounts of organic matter, typically ranging from 2 to 70 mg C·L^{-1} [81]. Similar concentrations have been observed before [82], but also higher > 100 mg C·L^{-1} [83,84] or very low < 2 mg C·L^{-1} [28,85], depending on the strain, and the culturing conditions.

3.2.1 Analysis of AOM

The AOM in the exponential and stationary phase had negative ζ, ranging from -10.3 to -26.3 mV for pH 4 to pH 10 (**Fig. A.3A**). The most positive value was recorded for pH 4 at approximately -12 mV, then plateaued at approximately -20 mV. It has been previously reported that the ζ constantly decreases as a function of pH and reaches -35 mV at pH 10 for exponential phase AOM with 9 mg·L^{-1} C, while it remains stable at -22 mV in the stationary phase between pH 4-10 [82,86].

Acid-base titrations indicated a difference in acid-base functionality between the cell growth phases (**Fig. A.4**). There was a major deprotonation at pH 6.6 and 5.6, resulting in a pK_a of approximately 2.7 and 3.2 for the exponential and stationary phases, respectively. This has been previously attributed to carboxyl groups. Above this pK_a, most of these functional groups will be negatively charged (-COO$^-$). However, in the stationary phase, a second equivalence point is observed at pH 9.0, with a pK_a of 8.2 [17,19,78], and required almost four times more (0.62 ± 0.03 mmol) OH^- to adjust the pH from 6.5 to 8. This experiment showed that a larger amount of acidic groups on a molar basis was present in the AOM in the stationary phase.

Further analysis on the dry AOM showed that the exponential phase was lower in C and higher in N concentration, with 24.7 ± 0.2% and 30.4 ± 3.2% $w \cdot w^{-1}$ dissolved organic carbon (DOC), and 1.5 ± 0.0% and 0.6 ± 0.0% $w \cdot w^{-1}$ DTN in dry AOM for the exponential and stationary phase, respectively (**Table 2**). This resulted in around 32.4 and 105.4 mg $AOM \cdot L^{-1}$ for the exponential and stationary phases, respectively.

Table 2. Determination of DOC, DTN, protein, total monosaccharides, and total SO_4^{2-} for the dialyzed (>1 kDa) AOM in dry weight basis % in the exponential and stationary growth phase.

Growth phase	Exponential	Stationary
Dissolved organic carbon (%)	24.7 ± 0.2	30.4 ± 3.2
Dissolved total nitrogen (%)	1.53 ± 0.01	0.61 ± 0.02
Protein (%)	9.1 ± 2.2	0.9 ± 0.2
Total monosaccharides (%)	15.1 ± 3.1	23.3 ± 1.1
Total SO_4^{2-} (%)	2.7 ± 0.2	0.6 ± 0.1

Accordingly, the exponential phase was ten times richer in proteins with 9.1 ± 2.2%, and reduced to 0.9 ± 0.2% $w \cdot w^{-1}$ in the stationary phase, corresponding to 2.9 ± 0.7 $mg \cdot L^{-1}$ and 0.9 ± 0.2 $mg \cdot L^{-1}$ protein in culture, respectively (**Table 2**). Green microalgae cultures have reported the existence of glycoproteins in the AOM [23,87], yet proteins and protein-like compounds are more pronounced in cyanobacterial cultures [78,88]. Usually, an accumulation of proteins in the AOM is observed (~1 up to 70 $mg \cdot L^{-1}$), but this is in contrast with the findings of this study, where the total amount of proteins decreased, indicating protein catabolism [23,82–85,88], and cannot explain the different influence in the exponential and stationary phase.

On the other hand, total monosaccharide content increased from exponential to stationary phase, and also were the leading major component for both growth phases, 15.1 ± 2.2% and 23.3 ± 1.1% $w \cdot w^{-1}$ for the exponential and stationary phases, respectively (**Table 2**). This corresponds to a concentration of 4.9 ± 1.0 $mg \cdot L^{-1}$ and 24.6 ± 1.2 $mg \cdot L^{-1}$, respectively. These values are within range of what is found in the literature for *Chlorella* species [23,24,82,84,85].

Polysaccharides (lectins) can bind with proteins to create a stable AOM matrix network and bridge cells with the rest of the AOM. Additionally, polysaccharides are known to be "highly hydrated hydrophilic" molecules and are mostly polyanionic due to uronic acid residues and occasionally because of ketal-linked pyruvate or sulfate, which can chemisorb to the cells surface [26,89], while polycationic polysaccharides with N-acetylglucosamine are rare [89].

Low MW proteins are known to inhibit coagulation due to their medium charge density and are reported to make metal complexes [24,26,27], while high MW proteins (>500 kDa) create a gel-like network with large polysaccharides, which enhances cell separation [24,82]. These suprastructures of coagulant-AOM-cell support separation [90], and it requires the abundance of polysaccharides and the presence of a low concentration of protein to act as a coagulant aid [53]. Overall, the clear decrease in the protein and increase in the monosaccharide content might be connected with the absence of inhibition in the stationary phase. Additionally, polysaccharides showcase different properties depending on their monomers and can affect cell aggregation, foaming, flocculation, cell adhesion, and more [87]. In this study, the exponential phase AOM was richer in arabinose (29.2±6.9%) and galactose (34.2±8.1%), with arabinose being the primary monosaccharide in the stationary phase (33.0±1.7%) (**Fig. 3**). In various instances, for *Chlorella* sp., galactose is the primary monosaccharide, followed by either arabinose, mannose, or fucose, with the presence [91] or absence of uronic acids [23]. In other reports, glucose stands out as the primary monosaccharide, often followed by arabinose or xylose and, subsequently, glucuronic acid [87]. Notably, in the stationary phase, glucosamine is no longer detected, or it could have coeluted with galactose, and the uronic acids have increased, but not significantly, with glucuronic acid at 5.92±3.6%.

Overall, the acidic sugars amounted to 6.7±2.1 and 13.1±5.8% of the total area of the chromatogram in the for the exponential and stationary phases, respectively, which might indicate that AOM in the stationary phase plays the role of coagulant aid for the interconnection of the constituents and gelling and foaming effects [91], and can explain the increase of OH^- equivalents during titration (**Fig. A.4**). Interestingly, uronic acids concentration has been observed to decrease during growth [25], possibly due to phosphate limitation [91]. Different types of stress respond in different polysaccharide composition [91]. Overall, the literature demonstrates a high percentage of charged hydrophilic components, hence elevated levels of acidic polysaccharides are expected (more than 60% of the AOM [81]), accompanied by increased intracellular and structural compounds due to cell lysis [17,92,93].

Furthermore, several unidentified monosaccharides remain in the neutral and acidic region. In the neutral region, some candidates could be 2-Deoxy-Glucose or Maltitol, and N-acetyl-glucosamine. In the acidic region, possible candidates are different uronic acids that are monocarboxylated sugars at the C6 carbon. Less likely acidic monosaccharides can be sulfated, phosphorylated, or they could even be sialic acids. However, total sulfate groups are decreasing from 2.7 ± 0.2% in the exponential phase to 0.6 ± 0.1% $w \cdot w^{-1}$ in the stationary phase AOM, corresponding to 0.9 ± 0.1 $mg \cdot L^{-1}$ and 0.7 ± 0.1 $mg \cdot L^{-1}$ sulfate group in culture, respectively. This does not indicate increased sulfated molecules, normally polysaccharides, in stationary phase to improve gelling characteristics [91] and foam formation.

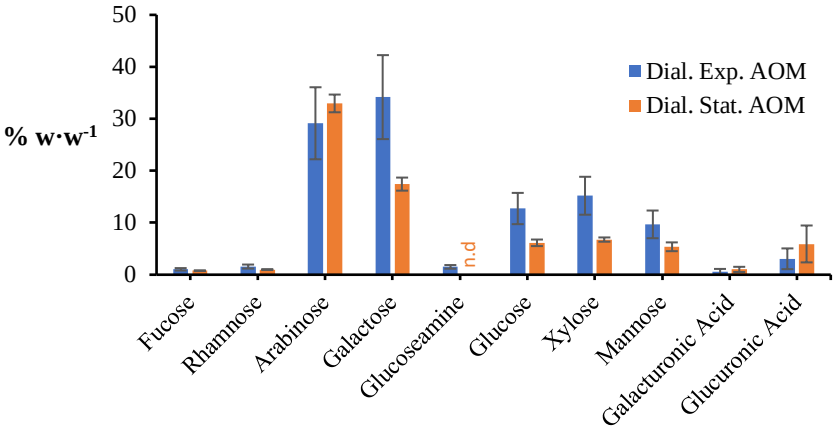

Figure 3. Monosaccharide composition of the identified and quantified monosaccharides in regards to the total monosaccharide quantification *via* the MBTH method. In the stationary phase, only 77.4% of monosaccharides were quantified. (Dial. Stat. AOM in duplicate). n.d. not detected

The polysaccharide-rich profile can also be seen in the FTIR spectra by firstly the broad peak of hydroxyl stretching at 3600-3000 cm^{-1} and two peaks at ~ 2936 and 2850 cm^{-1} for C-H stretching from -CH_2 axial deformation (**Fig. A.4**). Secondly, it is possible to see the water bending vibration at ~1632 cm^{-1}, and the CH and CH_2 bending at 1420 cm^{-1} [94]. Thirdly, the 1373 cm^{-1} signal could be the side chain vibration (CH_2-OH) [94]. Finally, typical signals can be identified in the fingerprint region of the FTIR spectra from 1150 to 760 cm^{-1}. The intense signals can be assigned to C-O and C-C vibrations (1145 -1080 cm^{-1} shoulder peak) and bending of C-O-H at 1037 cm^{-1}[94], C-O-C bending mode of anhydroglucose ring (~929, 897, 763 cm^{-1}) [95], and specifically the 897 cm^{-1} band can be connected to glycosidic linkages C1-H bending [66]. Overall, as expected, the polysaccharide signals in the stationary phase AOM spectrum appear more intense than the exponential phase AOM. Furthermore, the signal ~1725 cm^{-1} could be associated with carboxyl groups or esters. Carboxyl groups can be found on the

uronic acid residues, yet the signal at ~3300 cm^{-1} (OH) cannot be considered wide enough to confirm this, indicating the existence of esters.

In recent literature, the idea of an AOM network has become a recurring concept [24], following the principles of a biofilm. More recently, Cheng et al. [53] has shown microscope photos of captured *M. flos-aquae* cells in a network of aluminum-modified bubbles and AOM. Yet, proof of the AOM network, in the presence or absence of positively charged chemicals, should also be showcased *via* its mechanical properties (viscosity, surface tension, streamline flow, etc.) that are ultimately connected to its structure [87]. Hence, during the growth of *Chlorella* sp., AOM accumulates and changes, causing a profound impact on coagulation or successful attachment of aggregates with air bubbles in the stationary phase.

3.3 AOM in stationary phase improves separation efficiency in the absence of chitosan.

Thirdly, for the culture in the stationary phase in the presence of AOM (Stat.AOM+) the η was higher than 35%, without any coagulant dosing. This is rather unexpected, since the ζ of the culture was below -40 mV at pH ~8 (**Fig. 1B**), which aligns with previously reported values for *Chlorella* sp. cells [96]. Further, the ζ of the AOM was around -18 mV at pH 7-8 , and the air bubbles' ζ has been reported to vary around -40 mV at pH 7 [13]. Hence, the ζ indicates repulsive behavior, while the surprising increase in separation efficiency hints at the existence of interactions of different nature, like hydrophobic interactions, among cells, AOM, and bubbles. Distinctively, in the absence of AOM in the stationary phase (Stat.AOM-), η was below 20% (**Fig. 1A**). Thus, this suggests that the AOM in the stationary phase is different than in the exponential phase, and that it also affected the attachment of the cells to the bubbles, even in the absence of coagulant.

Imaging of the cells (unwashed) using the Quantitative Imaging (QI) mode of AFM showed that cells were enwrapped in AOM mucilage (**Fig. 4**) and that repetitive washing was essential to remove the majority of the AOM, with some tightly-bound residuals on the cell surface. Zoomed-in (1 μm × 1 μm) AFM height images were recorded on top of cells showing a 3-fold increase in average roughness from 1.3 ± 0.4 nm for the washed cells to 4.2 ± 2.4 nm for the unwashed cells (**Fig 4C, D, E**). This increase in roughness probably results from a heterogenous distribution of AOM on the cell surface (**Fig 4B, D**). The surface of the washed cells looks more homogenous (**Fig 4A, C**). In addition, the Young's modulus (Ym) was extracted by the force curves recorded on top of the cells in the force spectroscopy mode. For

the washed cells the Ym was 1474 ± 1053 kPa and 8 ± 10 kPa for the unwashed cells (**Fig. 4F, G)**. This pronounced difference can be explained by the presence of AOM around the unwashed cells, that creates a soft gel-like structure [97], forming the contact point upon indentation. In the case of washed cells, little AOM is present, thus the AFM tip directly enters in contact with the cell wall, which is more rigid (180 times) (all results are presented in **Table A.3**).

The presence of AOM around the cells in stationary phase triggered the question whether it improved bubble-cell attachment in the Stat.AOM+ conditions compared to the Stat.AOM-, when no chitosan is added. Hydrophobicity measurements with the FluidFM between cells and bubble showed that the mucilage of AOM around the cells had hydrophobic properties (**Fig. 5)**. Specifically, washed cells, presentative of the Stat.AOM- condition, did not interact with the air bubble for 90% of the force curves, while the rest interacted with low adhesion forces of 0.8 nN. This indicates that the cell wall is hydrophilic, while weak adhesions could be due to the small amount of tightly bound AOM on the cell surface. In the case of unwashed cells, representative of the Stat.AOM+ condition, heterogeneous results were obtained from the FluidFM experiments, but 64% of the force curves recorded interaction with the air bubble with an adhesion force of 2.5 ± 2.1 nN. This indicates that a significant portion of the AOM functionalities favors hydrophobic interactions with the air bubbles. From the bimodal adhesion characteristics observed for the unwashed cells, it can be inferred that one mode results from measurements conducted directly on the cell wall surface (which is completely hydrophilic), while the second one results from measurements at AOM-coated spots, providing its hydrophobic characteristics (all results are presented in **Table A.3**). The FTIR spectra, indeed, show an apparent increase at 1725 cm^{-1} of C=O ester stretching, also possibly connected to the 1247 cm^{-1} signal C-O stretching, while the rest C-O stretching vibrations of the ester group are overlapping with the polysaccharide signal about 1160 and 1050 cm^{-1} (**Fig. A.4**)[98]. Furthermore, there is a subtler shoulder left of the 2936 cm^{-1} peak which corresponds to CH_2 stretching of esterified fatty acids. The pyrolysis GC/MS of dichloromethane extracted AOM from the stationary phase confirmed the presence of nonpolar molecules with long aliphatic ester chains and aromatic rings (**Table A.4**).

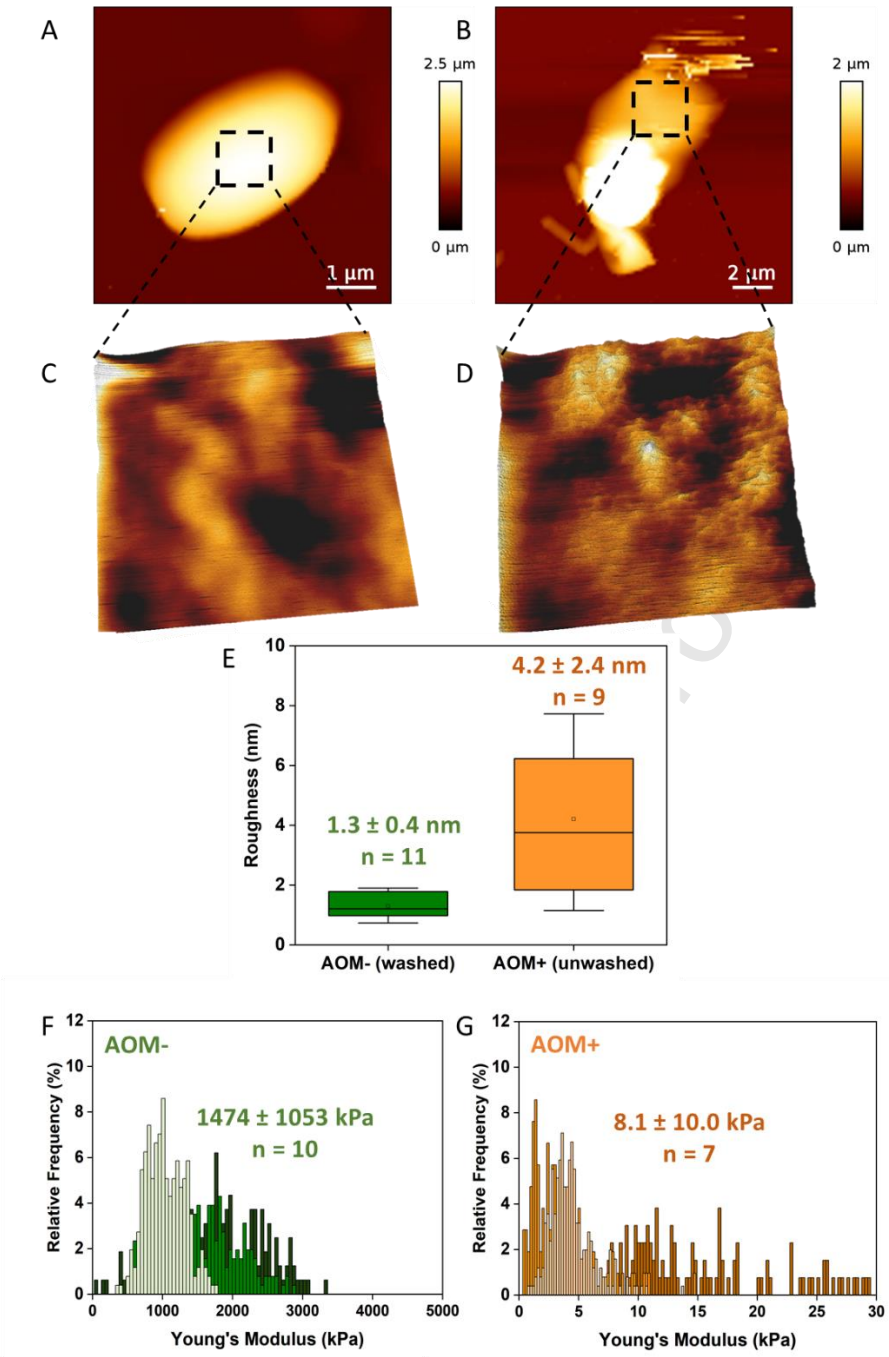

Figure 4. Biophysical properties of the *Chlorella* sp. cell surface in the stationary phase, when washed (little AOM) and unwashed (presence of AOM). Whole washed (A) and unwashed (B) cells were imaged by AFM. The 3-D zoom ins (1 µm × 1 µm) of the height images of the washed (C) and unwashed (D) cell surface. Average roughness (Ra) of washed and unwashed cells (E) and Young's Modulus were recorded on an area of 1×1 µm on top of the washed cells (F) (the shade of the green represent different single cells and only 3 cells were represented in the histogram however the average standard deviations were calculated from 10 different cells) and unwashed cells (G) (the shade of the orange represent different single cells and only 3 cells were represented in the histogram however the average and standard deviations were calculated from 7 different cells).

Washed cells from the exponential growth phase have been previously imaged and characterized [59]. No tightly bound AOM on the cell surface were observed after a two-step

washing protocol. This could mean that young cells carry fewer or different compounds on their surfaces that are not firmly attached to the cell wall. Furthermore, the exponential phase cells were also found to be hydrophilic (0% of adhesion with the air bubble interface) with comparable cells wall rigidity (1488 ± 408.8 kPa), yet with slightly decreased surface roughness (2.1 ± 0.5 nm). This contrasts with reported literature where cell wall rigidity has increased during culture growth [62,99], and has also been found to exhibit hydrophobic interactions [60].

Variety in the cell surface's characteristics and hydrophobicity are linked to the cell wall composition which depends on species, culture conditions and growth phase. The cell wall has been reported to be rich in proteins and carbohydrates [100] in the exponential phase, with the carbohydrate [101,102] or the lipid fraction [62] increasing during their growth at the expense of the protein fraction. Furthermore, the *Chlorella* genus is known for its diversity in cell wall polysaccharides [103], and thus cell wall characteristics. Indeed, cell wall polysaccharides show great variation for uronic acids, neutral, and amino sugars ratios, mostly with the principal monosaccharides being the neutral sugars rhamnose, galactose, and glucose [100,101]. Hence, the current *Chlorella* sp. cell wall would be expected to consist of hydrophilic polysaccharides [102] and proteins, and not lipid-containing molecules. Additionally, *Chlorella* sp. cells have been reported in different studies to have either a "chitosan-like layer" linked to glucosamine [101], or chitin-like and cellulose-like polysaccharides [104], or in some other cases a mannan cell wall [102].

On the other hand, hydrophobic compounds are expected to be present in the AOM, which forms a soft layer around the stationary phase cells. In the exponential phase, the AOM has been shown to form tightly packed micro-flocs with the *C. vulgaris* cells, while in the stationary phase, the cells and AOM has been shown to have an extended net formation (accumulated AOM and increased polysaccharide content) [101]. Furthermore, the AOM surrounding the cells could potentially change the apparent traits of the cell [93], increase the radius of gyration, and act as a flocculant aid [26], and facilitate interactions with the bubbles *via* hydrophobic interactions. Thus, it can be presumed that in the stationary phase, the AOM effect is not localized to a single or a small group of cells, but it is spread, possibly presenting hydrophobic traits to a larger area of the culture.

Overall, AFM showed that the *Chlorella* sp. cells carry a substantial amount of AOM in the stationary phase, which is challenging to remove. The AOM has biophysical characteristics different from those of the cell wall; it is softer and rougher and presents hydrophobic

properties. Hence, these results suggest that bound AOM and concentration of dissolved AOM played a critical role in the improved separation in the absence of chitosan.

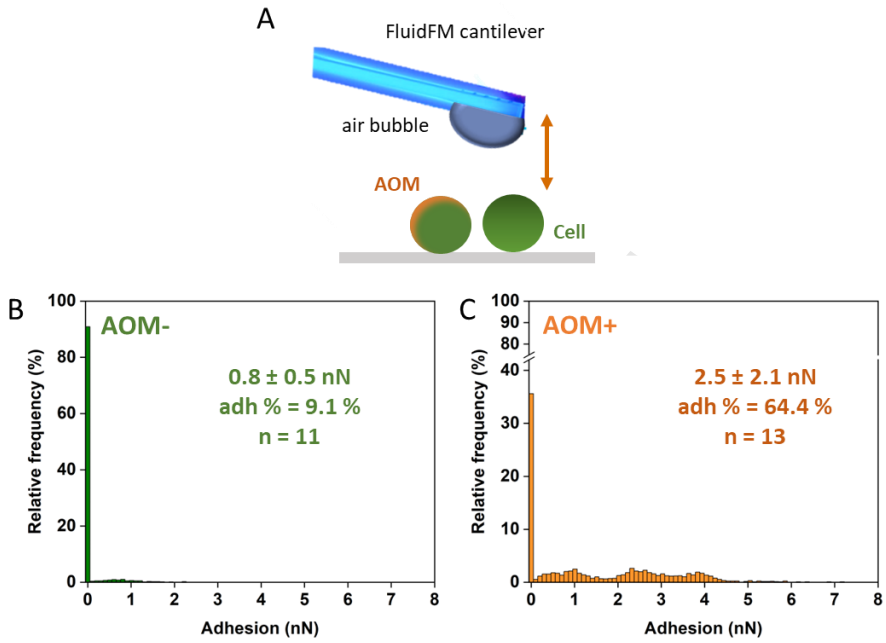

Figure 5. The cell adhesion to the bubble was measured *via* FluidFM at pH 7.4 (A). Only 9.1% of the cells interacted for AOM- (B) while 64.4% of the cells interacted for AOM+ (C). The average and standard deviations are annotated on the graphs.

4 Conclusions

The freshwater green microalgae *Chlorella* sp. culture was evaluated for chitosan coagulation and dissolved air flotation separation in exponential and stationary growth phase. High separation efficiencies were attainable for all tested treatments. In the absence of algal organic matter (AOM), there are small differences in chitosan coagulant demand between the exponential and the stationary phase; however, achieving high efficiency in the presence of AOM required nearly two times more coagulant in the exponential phase than the stationary phase, even though the culture had 3-4 times less AOM in dissolved organic carbon. In the stationary phase, the cells bear a substantial amount of AOM that alters their apparent characteristics, forming a soft layer of organic matter that can have complex and hydrophobic interactions with the bubble-air interface and extend its reach to other constituents. Furthermore, there is an accumulation of AOM rich in polysaccharides, consisting of primarily arabinose monosaccharide units followed by galactose, while acidic units are also present. These characteristics might facilitate the separation efficiency via chitosan coagulation-

flotation, while connecting the AOM composition to their structure and functionalities remains challenging.

Acknowledgements

We would like to acknowledge the technicians' support of Guy Reggers, Jenny Put, Elsy Thijssen, Martine Vanhamel, Bernard Noppen for TGA analyses, Ion Chromatography, HPAEC-PAD, FTIR, and PY-GC/MS.

Funding

This work was supported by Research Foundation Flanders (FWO junior fundamental research project - G050220N, FWO scientific exchange program Tournesol - VS01322N).

Appendix A. Supplementary data

References

[1] M.J. Barbosa, R.H. Wijffels, M. Janssen, C. Südfeld, S.D. Adamo, Hypes, hopes, and the way forward for microalgal biotechnology, Trends Biotechnol. 41 (2023). https://doi.org/10.1016/j.tibtech.2022.12.017.

[2] UN Environment, Global Environmental Outlook - GEO-6: Healthy Planet, Healthy People, Cambridge University Press, Nairobi, 2019. https://doi.org/10.1017/9781108627146.

[3] G.P. 't Lam, M.H. Vermuë, M.H.M. Eppink, R.H. Wijffels, C. van den Berg, Multi-Product Microalgae Biorefineries: From Concept Towards Reality, Trends Biotechnol. 36 (2018) 216–227. https://doi.org/10.1016/j.tibtech.2017.10.011.

[4] I. Gifuni, A. Pollio, C. Safi, A. Marzocchella, G. Olivieri, Current Bottlenecks and Challenges of the Microalgal Biorefinery, Trends Biotechnol. 37 (2019) 242–252. https://doi.org/10.1016/j.tibtech.2018.09.006.

[5] K. Muylaert, A. Beuckels, O. Depraetere, I. Foubert, G. Markou, D. Vandamme, Wastewater as a Source of Nutrients for Microalgae Biomass Production, in: N.R. Moheimani, M.P. McHenry, K. de Boer, P.A. Bahri (Eds.), Biomass Biofuels from Microalgae Adv. Eng. Biol., Springer International Publishing, Cham, 2015: pp. 75–94. https://doi.org/10.1007/978-3-319-16640-7_5.

[6] S. Li, T. Hu, Y. Xu, J. Wang, R. Chu, Z. Yin, F. Mo, L. Zhu, A review on flocculation as an efficient method to harvest energy microalgae: Mechanisms, performances, influencing factors and perspectives, Renew. Sustain. Energy Rev. 131 (2020) 110005. https://doi.org/10.1016/j.rser.2020.110005.

[7] F. Roselet, D. Vandamme, K. Muylaert, P.C. Abreu, Part II Microalgae for Biofuel Production, in: A. Alam, Z. Wang (Eds.), Microalgae Biotechnol. Dev. Biofuel Wastewater Treat., 2019: pp. 211–244.

[8] K.H. Min, D.H. Kim, M.R. Ki, S.P. Pack, Recent progress in flocculation, dewatering, and drying technologies for microalgae utilization: Scalable and low-cost harvesting process development, Bioresour. Technol. 344 (2022) 126404. https://doi.org/10.1016/j.biortech.2021.126404.

[9] J. Phasey, D. Vandamme, H.J. Fallow, Harvesting of algae in municipal wastewater treatment by calcium phosphate precipitation mediated by photosynthesis, sodium hydroxide and lime, Algal Res. 27 (2017) 115–120. https://doi.org/10.1016/j.algal.2017.06.015.

[10] M. Al-Sahari, A.A.S. Al-Gheethi, R.M.S.R. Mohamed, Natural Coagulates for Wastewater Treatment; A Review for Application and Mechanism, in: A.A.S. Al-gheethi, R.M.S.R. Mohamed, E.A. Noman, A. hashim M. Kassim (Eds.), Prospect. Fresh Mark. Wastes Manag. Dev. Ctries., 2020: pp. 17–32.

[11] A.L. Ahmad, M. Yasin, N. Hidayah, C. Derek, J. Lim, Optimization of microalgae coagulation process using chitosan, Chem. Eng. J. 173 (2011) 879–882. https://doi.org/10.1016/j.cej.2011.07.070.

[12] G. Chen, L. Zhao, Y. Qi, Y. Cui, Chitosan and Its Derivatives Applied in Harvesting Microalgae for Biodiesel Production: An Outlook, J. Nanomater. 2014 (2014).

[13] Y. Wang, W. Sun, L. Ding, W. Liu, L. Tian, Y. Zhao, M. Zhang, X. Wang, A study on the feasibility and mechanism of enhanced co-coagulation dissolved air flotation with chitosan-modified microbubbles, J. Water Process Eng. 40 (2021) 1–11.

[14] F.H.M. Yunos, N.M. Nasir, H.H.W. Jusoh, H. Khatoon, S.S. Lam, A. Jusoh, Harvesting of microalgae (Chlorella sp.) from aquaculture bioflocs using an environmental-friendly chitosan-based bio-coagulant, Int. Biodeterior. Biodegradation 124 (2017) 243–249. https://doi.org/10.1016/j.ibiod.2017.07.016.

[15] S. Bhalkaran, L.D. Wilson, Investigation of Self-Assembly Processes for Chitosan-Based Coagulant-Flocculant Systems: A Mini-Review, Int. J. Mol. Sci. 17 (2016) 1662. https://doi.org/10.3390/ijms17101662.

[16] I. Agerkvist, Mechanisms of flocculation with chitosan in Escherichia coli disintegrates: effects of urea and chitosan characteristics, Colloids and Surfaces 173 (1992) 173–187.

[17] X. Zang, H. Zhang, Q. Liu, L. Li, L. Li, X. Zhang, Harvesting of Microcystis flos-aquae using chitosan coagulation: Influence of proton-active functional groups originating from extracellular and intracellular organic matter, Water Res. 185 (2020). https://doi.org/10.1016/j.watres.2020.116272.

[18] J. Blockx, A. Verfaillie, W. Thielemans, K. Muylaert, Unravelling the Mechanism of Chitosan-Driven Flocculation of Microalgae in Seawater as a Function of pH, ACS Sustain. Chem. Eng. 6 (2018) 11273–11279. https://doi.org/10.1021/acssuschemeng.7b04802.

[19] S. Cheng, H. Zhang, L. Li, T. Yu, Y. Wang, D. Tan, X. Zhang, Harvesting of Microcystis flos-aquae using dissolved air flotation: The inhibitory effect of carboxyl groups in uronic acid-containing carbohydrates, Chemosphere 300 (2022) 134466. https://doi.org/10.1016/j.chemosphere.2022.134466.

[20] I. Demir, J. Blockx, E. Dague, P. Guiraud, W. Thielemans, K. Muylaert, C. Formosa-Dague, Nanoscale Evidence Unravels Microalgae Flocculation Mechanism Induced by Chitosan, ACS Appl. Bio Mater. 3 (2020) 8446–8459. https://doi.org/10.1021/acsabm.0c00772.

[21] Y. Gerchman, B. Vasker, M. Tavasi, Y. Mishael, Y. Kinel-tahan, Effective harvesting of microalgae: Comparison of different polymeric flocculants, Bioresour. Technol. 228 (2017) 141–146. https://doi.org/10.1016/j.biortech.2016.12.040.

[22] R.K. Henderson, S.A. Parsons, B. Jefferson, The impact of differing cell and algogenic organic matter (AOM) characteristics on the coagulation and flotation of algae, Water Res. 44 (2010) 3617–3624. https://doi.org/10.1016/j.watres.2010.04.016.

[23] N.R.H. Rao, A.M. Granville, P.R. Wich, R.K. Henderson, Detailed algal extracellular carbohydrate-protein characterisation lends insight into algal solid-liquid separation process outcomes, Water Res. 178 (2020) 115833. https://doi.org/10.1016/j.watres.2020.115833.

[24] N.R.H. Rao, A.M. Granville, R.K. Henderson, Understanding variability in algal solid-liquid separation process outcomes by manipulating extracellular protein-carbohydrate interactions, Water Res. 190 (2021) 116747. https://doi.org/10.1016/j.watres.2020.116747.

[25] O. Hoyer, B. Lüsse, H. Bernhardt, lsolation and characterization oĺ extracellular organic matter (EOM) from algae, Zeitschrift Für Wasser- Und Abwasser-Forsch. 18 (1985) 76–90.

[26] H. Bernhardt, O. Hoyer, H. Schell, B. Lüsse, Reaction mechanisms involved in the influence of algogenic organic matter on flocculation, Zeitschrift Für Wasser- Und Abwasser-Forsch. 18 (1985) 18–30.

[27] M. Pivokonsky, J. Safarikova, P. Bubakova, L. Pivokonska, Coagulation of peptides and proteins produced by Microcystis aeruginosa: Interaction mechanisms and the effect of Fe-peptide/protein complexes formation, Water Res. 6 (2012) 3–10.

[28] R.K. Henderson, S.A. Parsons, B. Jefferson, The impact of differing cell and algogenic organic matter (AOM) characteristics on the coagulation and flotation of algae, Water Res. 44 (2010) 3617–3624. https://doi.org/10.1016/j.watres.2010.04.016.

[29] C.A. Laamanen, G.M. Ross, J.A. Scott, Flotation harvesting of microalgae, Renew. Sustain. Energy Rev. 58 (2016) 75–86. https://doi.org/10.1016/j.rser.2015.12.293.

[30] A.F. Esteves, C.J. Almeida, A.L. Gonçalves, J.C. Pires, Microalgae harvesting techniques, in: E. Jacob-Lopes, M.M. Maroneze, M.I. Queiroz, L.Q.B.T.-H. of M.-B.P. and P. Zepka (Eds.), Handb. Microalgae-Based Process. Prod., Academic Press, 2020: pp. 225–281. https://doi.org/https://doi.org/10.1016/B978-0-12-818536-0.00010-5.

[31] H. Zhang, X. Zhang, Microalgal harvesting using foam flotation: A critical review, Biomass and Bioenergy 120 (2019) 176–188. https://doi.org/10.1016/j.biombioe.2018.11.018.

[32] N. Rajapakse, M. Zargar, T. Sen, M. Khiadani, Effects of influent physicochemical characteristics on air dissolution, bubble size and rise velocity in dissolved air flotation: A review, Sep. Purif. Technol. 289 (2022) 120772.

[33] J.K. Edzwald, Dissolved air flotation and me, Water Res. 44 (2010) 2077–2106. https://doi.org/10.1016/j.watres.2009.12.040.

[34] S.L. Pahl, A.K. Lee, T. Kalaitzidis, P.J. Ashman, S. Sathe, D.M. Lewis, Harvesting, Thickening and Dewatering Microalgae Biomass, in: M.A. Borowitzka, N.R. Moheimani (Eds.), Algae for Biofuels and Energy, 5th ed., Springer Science+Business Media, Dordrecht, 2013: pp. 165–185. https://doi.org/10.1007/978-94-007-5479-9.

[35] J.K. Edzwald, Dissolved air flotation and me, Water Res. 44 (2010) 2077–2106. https://doi.org/10.1016/j.watres.2009.12.040.

[36] S.F. Han, W. Jin, R. Tu, S.H. Gao, X. Zhou, Microalgae harvesting by magnetic flocculation for biodiesel production: current status and potential, World J. Microbiol. Biotechnol. 36 (2020) 1–10. https://doi.org/10.1007/s11274-020-02884-5.

[37] Z. Yang, J. Hou, L. Miao, Harvesting freshwater microalgae with natural polymer flocculants, Algal Res. 57 (2021) 102358. https://doi.org/10.1016/j.algal.2021.102358.

[38] A. Verfaillie, J. Blockx, K. Muylaert, R. Praveenkumar, W. Thielemans, Harvesting of marine microalgae using cationic cellulose nanocrystals, Carbohydr. Polym. 240 (2020).

[39] H. Salehizadeh, N. Yan, R. Farnood, Recent advances in polysaccharide bio-based flocculants, Biotechnol. Adv. 36 (2018) 92–119. https://doi.org/10.1016/j.biotechadv.2017.10.002.

[40] B.T. Iber, V.T. Okomoda, S.A. Rozaimah, N.A. Kasan, Eco-friendly approaches to aquaculture wastewater treatment: Assessment of natural coagulants vis-a-vis chitosan, Bioresour. Technol. Reports 15 (2021) 100702. https://doi.org/10.1016/j.biteb.2021.100702.

[41] S. Rossi, S. Visigalli, F. Castillo Cascino, M. Mantovani, V. Mezzanotte, K. Parati, R. Canziani, A. Turolla, E. Ficara, Metal-based flocculation to harvest microalgae: a look beyond separation efficiency, Sci. Total Environ. 799 (2021) 149395. https://doi.org/10.1016/j.scitotenv.2021.149395.

[42] W.M. Kedir, G.F. Abdi, M.M. Goro, L.D. Tolesa, Pharmaceutical and drug delivery applications of chitosan biopolymer and its modified nanocomposite: A review, Heliyon 8 (2022) e10196. https://doi.org/10.1016/j.heliyon.2022.e10196.

[43] European Commission, Food and Feed Information Portal Database _ Chitosan, Comm. Regul. 432/2012 (2012). https://ec.europa.eu/food/food-feed-portal/screen/novel-food-catalogue/search%0Ahttps://ec.europa.eu/food/food-feed-portal/screen/feed-additives/search.

[44] P. Baldrick, The safety of chitosan as a pharmaceutical excipient, Regul. Toxicol. Pharmacol. 56 (2010) 290–299. https://doi.org/10.1016/j.yrtph.2009.09.015.

[45] I. Aranaz, A.R. Alcántara, M.C. Civera, B. Elorza, A.H. Caballero, N. Acosta, Chitosan: An Overview of Its Properties and Applications, Polymers (Basel). 13 (2021) 3256.

[46] C.N. Ogbonna, E.G. Nwoba, Bio-based flocculants for sustainable harvesting of microalgae for biofuel production. A review, Renew. Sustain. Energy Rev. 139 (2021) 110690. https://doi.org/10.1016/j.rser.2020.110690.

[47] H. Jethani, U.H. Hebbar, Plant-based biopolymers: emerging bio-flocculants for microalgal biomass recovery, Rev. Environ. Sci. Bio/Technology 20 (2021) 143–165. https://doi.org/10.1007/s11157-020-09561-x.

[48] M. Mucci, N.P. Noyma, L. de Magalhães, M. Miranda, F. van Oosterhout, I.A. Guedes, V.L.M. Huszar, M.M. Marinho, M. Lürling, Chitosan as coagulant on cyanobacteria in lake restoration management may cause rapid cell lysis, Water Res. 118 (2017) 121–130. https://doi.org/10.1016/j.watres.2017.04.020.

[49] G. Nam, M.M. Mohamed, J. Jung, Novel treatment of Microcystis aeruginosa using chitosan-modified nanobubbles, Environ. Pollut. 292 (2022) 118458. https://doi.org/10.1016/j.envpol.2021.118458.

[50] P. Guo, Y. Liu, C. Liu, Effects of chitosan, gallic acid, and algicide on the physiological and biochemical properties of Microcystis flos-aquae, Environ. Sci. Pollut. Res. 22 (2015) 13514–13521. https://doi.org/10.1007/s11356-015-4500-0.

[51] L. Zhu, Z. Li, E. Hiltunen, Microalgae Chlorella vulgaris biomass harvesting by natural flocculant: Effects on biomass sedimentation, spent medium recycling and lipid extraction, Biotechnol. Biofuels 11 (2018) 183. https://doi.org/10.1186/s13068-018-1183-z.

[52] D. Tang, H. Ji, L. Zhang, Effects of residual flocculants on cultivation of Auxenochlorella pyrenoidosa: Lipid production and transcriptomic insights, Bioresour. Technol. 422 (2025) 132249. https://doi.org/10.1016/j.biortech.2025.132249.

[53] S. Cheng, H. Zhang, H. Wang, M. Mubashar, L. Li, X. Zhang, Influence of the algal organic matter in the in-situ flotation removal of Microcystis using positively charged bubbles, Bioresour. Technol. 397 (2024) 130468. https://doi.org/10.1016/j.biortech.2024.130468.

[54] R. Rippka, J. Deruelles, J.B. Waterbury, M. Herdman, R.Y. Stanier, Generic Assignments, Strain Histories and Properties of Pure Cultures of Cyanobacteria, J. Gen. Microbiol. 110 (1979) 1–61.

[55] N.R. Moheimani, M.A. Borowitzka, A. Isdepsky, S. Fon Sing, Standard Methods for Measuring Growth of Algae and Their Composition, in: M.A. Borowitzka, N.R. Moheimani (Eds.), Algae for Biofuels and Energy, 5th ed., Springer Science+Business Media, Dordrecht, 2013: pp. 265–288. https://doi.org/10.1007/978-94-007-5479-9.

[56] W. Vercruysse, C.L. Gomes, D. Bleus, M. Pappa, B. Joos, A. Hardy, W. Marchal, D. Vandamme, Demineralization of common ivy-derived biomass and biochar and its effect on the resulting activated carbon properties, Sep. Purif. Technol. 319 (2023) 124023. https://doi.org/10.1016/j.seppur.2023.124023.

[57] N.R.H. Rao, A. Gonzalez-Torres, B. Tamburic, Y.W. Wong, I. Foubert, K. Muylaert, R.K. Henderson, D. Vandamme, The influence of physical floc properties on the separation of marine microalgae via alkaline flocculation followed by dissolved air flotation, Algal Res. 71 (2023) 103024. https://doi.org/10.1016/j.algal.2023.103024.

[58] S. Lama, K. Muylaert, T.B. Karki, I. Foubert, R.K. Henderson, D. Vandamme, Flocculation properties of several microalgae and a cyanobacterium species during ferric chloride, chitosan and alkaline flocculation, Bioresour. Technol. 220 (2016) 464–470. https://doi.org/10.1016/j.biortech.2016.08.080.

[59] I. Demir-Yilmaz, M. Pappa, S. Lama, P. Guiraud, D. Vandamme, C. Formosa-Dague, The Biophysical Properties of Microalgal Cell Surfaces Govern Their Interactions with an Amphiphilic Chitosan Derivative Used for Flocculation and Flotation, ACS Appl. Bio Mater. (2024). https://doi.org/10.1021/acsabm.4c00363.

[60] I. Demir-Yilmaz, M.S. Ftouhi, S. Balayssac, P. Guiraud, C. Coudret, C. Formosa-Dague, Bubble functionalization in flotation process improve microalgae harvesting, Chem. Eng. J. 452 (2023) 139349. https://doi.org/10.1016/j.cej.2022.139349.

[61] H. Hertz, Ueber die beruhrung fester elastischer korper, J. Für Die Reine Und Angew. Math. (1881) 156–171.

[62] I. Demir-Yilmaz, M. Schiavone, J. Esvan, P. Guiraud, C. Formosa-Dague, Combining AFM, XPS and chemical hydrolysis to understand the complexity and dynamics of C. vulgaris cell wall composition and architecture, Algal Res. 72 (2023). https://doi.org/10.1016/j.algal.2023.103102.

[63] I. Demir, I. Lüchtefeld, C. Lemen, E. Dague, P. Guiraud, T. Zambelli, C. Formosa-dague, Probing the interactions between air bubbles and (bio)interfaces at the nanoscale using FluidFM technology, J. Colloid Interface Sci. 604 (2021) 785–797. https://doi.org/10.1016/j.jcis.2021.07.036.

[64] J. Hutter, J. Bechhoefer, Calibration of Atomic-Force Microscope Tips, Rev. Sci. Instrum. 64 (1993) 1868–1873. https://doi.org/10.1063/1.1143970.

[65] W. Vercruysse, M. Pappa, G. Mangione, D. Desta, A. Hardy, H.G. Boyen, M.K. Van Bael, W. Marchal, D. Vandamme, Improving Nitrogen Retention in Algal Biochar Pyrolysis by Co-Pyrolysis with Glucose, Adv. Sustain. Syst. 7 (2023) 1–12. https://doi.org/10.1002/adsu.202300236.

[66] S. Lama, M. Pappa, N.B. Watanabe, C.F. Dague, W. Marchal, P. Adriaensens, D. Vandamme, Interference of extracellular soluble algal organic matter on flocculation-sedimentation harvesting of Chlorella sp, Bioresour. Technol. (2024) 131290. https://doi.org/10.1016/j.biortech.2024.131290.

[67] D. Fengel, G. Wegener, Hydrolysis of Polysaccharides with Trifluoroacetic Acid and its Application to Rapid Wood and Pulp Analysis, in: R.D. Brown (Ed.), Hydrolys. Cellul. Mech. Enzym. Acid Catal., American Chemical Society, 1979: pp. 145–158.

[68] S. Van Wychen, L.M.L. Laurens, Determination of Total Carbohydrates in Algal Biomass - Laboratory Analytical Procedure (LAP), Lab. Anal. Proced. (2015). www.nrel.gov/publications.

[69] S. Van Wychen, W. Long, S.K. Black, L.M.L. Laurens, MBTH: A novel approach to rapid, spectrophotometric quantitation of total algal carbohydrates, Anal. Biochem. 518 (2017) 90–93. https://doi.org/10.1016/j.ab.2016.11.014.

[70] A. Nagel, S. Sirisakulwat, R. Carle, S. Neidhart, An Acetate−Hydroxide Gradient for the Quantitation of the Neutral Sugar and Uronic Acid Profile of Pectins by HPAEC-PAD without Postcolumn pH Adjustment, J. Agric. Food Chem. 62 (2014) 2037–2048.

[71] K.S. Dodgson, R.G. Price, A Note on the Determination of the Ester Sulphate Content of Sulphated Polysaccharides, Biochem. J. 84 (1962) 106–110.

[72] K.S. Dodgson, Determination of Inorganic Sulphate in Studies on the Enzymic and Non-Enzymic Hydrolysis of Carbohydrate and Other Sulphate Esters, Biochem. J. 78 (1961) 312–319.

[73] H.L. Hardell, N.O. Nilvebrant, A rapid method to discriminate between free and esterified fatty acids by pyrolytic methylation using tetramethylammonium acetate or hydroxide, J. Anal. Appl. Pyrolysis 52 (1999) 1–14. https://doi.org/10.1016/S0165-

2370(99)00035-2.

[74] H. Zhang, C. Li, L. Li, S. Cheng, P. Wang, L. Sun, J. Huang, X. Zhang, Uncovering the optimal structural characteristics of flocs for microalgae flotation using Python-OpenCV, J. Clean. Prod. 385 (2023) 135748. https://doi.org/10.1016/j.jclepro.2022.135748.

[75] Y.S. Cheng, Y. Zheng, J.M. Labavitch, J.S. Vandergheynst, The impact of cell wall carbohydrate composition on the chitosan flocculation of Chlorella, Process Biochem. 46 (2011) 1927–1933. https://doi.org/10.1016/j.procbio.2011.06.021.

[76] H. Bernhardt, J. Clasen, Investigations into the flocculation mechanisms of small algal cells.pdf, Aqua- J. Water Supply Res. Technol. 43 (1994) 222–232.

[77] R.K. Henderson, S.A. Parsons, B. Jefferson, Successful Removal of Algae through the Control of Zeta Potential, Sep. Sci. Technol. 43 (2008) 1653–1666. https://doi.org/10.1080/01496390801973771.

[78] J. Safarikova, M. Baresova, M. Pivokonsky, I. Kopecka, Influence of peptides and proteins produced by cyanobacterium Microcystis aeruginosa on the coagulation of turbid waters, Sep. Purif. Technol. 118 (2013) 49–57. https://doi.org/http://dx.doi.org/10.1016/j.seppur.2013.06.049.

[79] S. Hadjoudja, V. Deluchat, M. Baudu, Cell surface characterisation of Microcystis aeruginosa and Chlorella vulgaris, J. Colloid Interface Sci. 342 (2010) 293–299. https://doi.org/10.1016/j.jcis.2009.10.078.

[80] X. Zhang, J.C. Hewson, P. Amendola, M. Reynoso, M. Sommerfeld, Y. Chen, Q. Hu, Critical evaluation and modeling of algal harvesting using dissolved air flotation., Biotechnol. Bioeng. 9999 (2014) 1–9. https://doi.org/10.1002/bit.25300.

[81] L. Zhuang, Y. Wu, V. Manuel, D. Espinosa, T. Zhang, G. Dao, H. Hu, Soluble Algal Products (SAPs) in large scale cultivation of microalgae for biomass/bioenergy production: A review, Renew. Sustain. Energy Rev. 59 (2016) 141–148. https://doi.org/10.1016/j.rser.2015.12.352.

[82] R.K. Henderson, A. Baker, S.A. Parsons, B. Jefferson, Characterisation of algogenic organic matter extracted from cyanobacteria, green algae and diatoms, Water Res. 42 (2008) 3435–3445. https://doi.org/10.1016/j.watres.2007.10.032.

[83] Z. Yu, H. Pei, Q. Hou, C. Nie, L. Zhang, Z. Yang, X. Wang, The effects of algal extracellular substances on algal growth, metabolism and long-term medium recycle, and inhibition alleviation through ultrasonication, Bioresour. Technol. 267 (2018) 192–200. https://doi.org/10.1016/j.biortech.2018.07.019.

[84] F. Zhao, Y. Su, X. Tan, H. Chu, Y. Zhang, L. Yang, Effect of temperature on extracellular organic matter (EOM) of Chlorella pyrenoidosa and effect of EOM on irreversible membrane fouling, Colloids Surfaces B Biointerfaces 136 (2015) 431–439.

[85] Y. Chiou, M. Hsieh, H. Yeh, Effect of algal extracellular polymer substances on UF membrane fouling, Desalination 250 (2010) 648–652. https://doi.org/10.1016/j.desal.2008.02.043.

[86] C. Matho, K. Schwarzenberger, K. Eckert, B. Keshavarzi, T. Walther, J. Steingroewer, F. Krujatz, Bio-compatible flotation of Chlorella vulgaris: Study of zeta potential and flotation efficiency, Algal Res. 44 (2019) 101705. https://doi.org/10.1016/j.algal.2019.101705.

[87] R. Xiao, Y. Zheng, Overview of microalgal extracellular polymeric substances (EPS) and their applications, Biotechnol. Adv. 34 (2016) 1225–1244. https://doi.org/10.1016/j.biotechadv.2016.08.004.

[88] M. Pivokonsky, J. Safarikova, M. Baresova, L. Pivokonska, I. Kopecka, A comparison of the character of algal extracellular versus cellular organic matter produced by cyanobacterium, diatom and green alga, Water Res. 51 (2014) 37–46. https://doi.org/10.1016/j.watres.2013.12.022.

[89] H. Flemming, J. Wingender, The biofilm matrix, Nat. Rev. Microbiol. 8 (2010) 623–633. https://doi.org/10.1038/nrmicro2415.

[90] R.K.L. Yap, M. Whittaker, M. Diao, R.M. Stuetz, B. Jefferson, V. Bulmus, W.L. Peirson, A. V Nguyen, R.K. Henderson, Hydrophobically-associating cationic polymers as micro-bubble surface modifiers in dissolved air flotation for cyanobacteria cell separation, Water Res. 61 (2014) 253–262. https://doi.org/10.1016/j.watres.2014.05.032.

[91] C. Laroche, Exopolysaccharides from Microalgae and Cyanobacteria: Diversity of Strains, Production Strategies, and Applications, Mar. Drugs 20 (2022) 336.

[92] W. Zhang, Q. Cao, G. Xu, D. Wang, Flocculation − Dewatering Behavior of Microalgae at Different Growth Stages under Inorganic Polymeric Flocculant Treatment: The Relationships between Algal Organic Matter and Floc Dewaterability, ACS Sustain. Chem. Eng. (2018) 11087–11096. https://doi.org/10.1021/acssuschemeng.8b02551.

[93] F. Sun, H. Zhang, A. Qian, H. Yu, C. Xu, R. Pan, Y. Shi, The influence of extracellular polymeric substances on the coagulation process of cyanobacteria, Sci. Total Environ. 720 (2020) 137573.

[94] V. Garces, A. García-Quintero, T.A. Lerma, M. Palencia, E.M. Combatt, Á.A. Arrieta, Characterization of Cassava Starch and Its Structural Changes Resulting of Thermal Stress by Functionally-Enhanced Derivative Spectroscopy (FEDS), Polysaccharides 2 (2021) 866–877. https://doi.org/10.3390/polysaccharides2040052.

[95] L.A. Castillo, O. V. López, M.A. García, S.E. Barbosa, M.A. Villar, Crystalline morphology of thermoplastic starch/talc nanocomposites induced by thermal processing, Heliyon 5 (2019). https://doi.org/10.1016/j.heliyon.2019.e01877.

[96] N. Li, P. Wang, S. Wang, C. Wang, H. Zhou, S. Kapur, J. Zhang, Y. Song, Electrostatic charges on microalgae surface: Mechanism and applications, J. Environ. Chem. Eng. 10 (2022) 107516. https://doi.org/10.1016/j.jece.2022.107516.

[97] J.B. Vergnes, V. Gernigon, P. Guiraud, C. Formosa-Dague, Bicarbonate Concentration Induces Production of Exopolysaccharides by Arthrospira platensis That Mediate Bioflocculation and Enhance Flotation Harvesting Efficiency, ACS Sustain. Chem. Eng.

7 (2019) 13796−13804. https://doi.org/10.1021/acssuschemeng.9b01591.

[98] A. Rohman, Y.B.C. Man, Fourier transform infrared (FTIR) spectroscopy for analysis of extra virgin olive oil adulterated with palm oil, Food Res. Int. 43 (2010) 886–892. https://doi.org/10.1016/j.foodres.2009.12.006.

[99] B.H.J. Yap, S.A. Crawford, R.R. Dagastine, P.J. Scales, G.J.O. Martin, Nitrogen deprivation of microalgae: effect on cell size, cell wall thickness, cell strength, and resistance to mechanical disruption, J. Ind. Microbiol. Biotechnol. 43 (2016) 1671–1680. https://doi.org/10.1007/s10295-016-1848-1.

[100] Y.-S. Cheng, J.M. Labavitch, J.S. Vandergheynst, Elevated CO2 concentration impacts cell wall polysaccharide composition of green microalgae of the genus Chlorella, Lett. Appl. Microbiol. 60 (2014) 1–7. https://doi.org/10.1111/lam.12320.

[101] G. Canelli, P.M. Martínez, S. Austin, M.E. Ambühl, F. Dionisi, C.J. Bolten, R. Carpine, L. Neutsch, A. Mathys, Biochemical and morphological characterization of heterotrophic crypthecodinium cohnii and chlorella vulgaris cell walls, J. Agric. Food Chem. 69 (2021) 2226–2235. https://doi.org/10.1021/acs.jafc.0c05032.

[102] O. Spain, C. Funk, Detailed Characterization of the Cell Wall Structure and Composition of Nordic Green Microalgae, J. Agric. Food Chem. 70 (2022) 9711–9721. https://doi.org/10.1021/acs.jafc.2c02783.

[103] H. Takeda, SUGAR COMPOSITION OF THE CELL WALL AND THE TAXONOMY OF CHLORELLA (CHLOROPHYCEAE), J. Phycol. 27 (1991) 224–232. https://doi.org/https://doi.org/10.1111/j.0022-3646.1991.00224.x.

[104] S. Weber, P.M. Grande, L.M. Blank, H. Klose, Insights into cell wall disintegration of Chlorella vulgaris, PLoS One 17 (2022) 1–14. https://doi.org/10.1371/journal.pone.0262500.

Highlights

1. 40% less chitosan was required in the stationary (day 20) compared to the exponential (day 6) growth phase.
2. Cells at day 20 had a layer of organic matter that could interact with air bubbles based on FluidFM experiments.
3. Stationary algal organic matter contained 23.3% polysaccharides of which more than 80% were neutral monosaccharides.
4. Stationary algal organic matter contained less than 1% of proteins.